Available online at www.sciencedirect.com
SCIENCE DIRECT®
Journal of Catalysis 220 (2003) 215–225
JOURNAL OF CATALYSIS
www.elsevier.com/locate/jcat

# Palladium–silver sol–gel catalysts for selective hydrodechlorination of 1,2-dichloroethane into ethylene
## IV. Deactivation mechanism and regeneration

Benoît Heinrichs,[a,*] Francis Noville,[a] Jean-Paul Schoebrechts,[b] and Jean-Paul Pirard [a]

[a] *Laboratoire de Génie Chimique, B6a, Université de Liège, B-4000 Liège, Belgium*
[b] *Laboratoire Central, Solvay, S.A., Rue de Ransbeek, 310, B-1120 Brussels, Belgium*

Received 27 February 2003; revised 7 July 2003; accepted 9 July 2003

**Abstract**

The activity and selectivity of a 1.9% Pd–3.7% $Ag/SiO_2$ catalyst during selective hydrodechlorination of 1,2-dichloroethane into ethylene have been followed in the course of time. The deactivation curves show two distinct periods: an initial period at the very beginning of catalyst operation, that is, during the first 20 operating hours, characterized by a sharp decrease of the rates of both reactions involved in the process (1,2-dichloroethane hydrodechlorination and undesired ethylene hydrogenation) and a second period, after the first 20 operating hours and investigated for more than 600 h, characterized by a clearly slower deactivation. During the initial period, the hydrodechlorination rate decreases less quickly than the hydrogenation rate and this results in a fast increase of ethylene selectivity which reaches a maximum at the end of this period. After the initial period, the hydrodechlorination rate decreases faster than the hydrogenation rate and this results in a slow decrease of ethylene selectivity. A comparison between the physico-chemical properties of the fresh catalyst and of the deactivated one suggests a deactivation mechanism by poisoning or coking of silver sites at the surface of the active Pd–Ag alloy particles whereas palladium sites would remain intact. The selectivity evolution during the second period, that is, after the very first operating hours, is in agreement with such a mechanism. However, the sharp ethylene selectivity increase during the initial operating hours suggests, in addition to the deactivation by silver sites disappearance, the presence of a further nonidentified phenomenon. The characterization of the catalyst after a regeneration treatment including an oxidation step followed by a reduction step shows that this treatment allows restoration near to the physico-chemical properties of the fresh catalyst.


*Keywords:* Hydrodechlorination; 1,2-Dichloroethane; Pd–Ag catalyst; Deactivation; Regeneration

## 1. Introduction

Catalysts lose frequently a large portion of their activity during operation. Three main causes are generally responsible for catalyst deactivation [1–3]: solid-state transformation in particular sintering of supported metal particles leading to a loss of active surface and sintering of the support leading to the disappearance of porosity and thus making active sites inaccessible; poisoning which results from an irreversible chemisorption of species from the gaseous or liquid phase on active sites; and coking that is the deposition of carbonaceous residues on active sites or inside the support porosity (fouling).

In the particular case of hydrodechlorination reactions over supported metal catalysts, the deactivation causes generally suggested are metal poisoning by chlorine [4–9], coking [5,6,10–18], metal sintering [8,19–21], and loss of metal due to formation of volatile chlorides [19].

In the present paper, the activity and selectivity temporal evolution of the cogelled sol–gel catalyst 1.9% Pd–3.7% $Ag/SiO_2$, named Pd–Ag (33–67) in the previous papers of this series [22–24], as well as its physico-chemical properties before operation in the hydrodechlorination reactor (fresh catalyst already characterized in [22] and [23]), after operation (deactivated catalyst) and after a regeneration treatment (regenerated catalyst) are described in detail. This study has a double purpose: on the one hand, by means of ex-

* Corresponding author.
*E-mail address:* b.heinrichs@ulg.ac.be (B. Heinrichs).

0021-9517/$ – see front matter 
doi:10.1016/j.jcat.2003.07.006

perimental data, to find the possible deactivation causes, and on the other hand, to examine the efficiency of the treatment proposed for regeneration.

## 2. Experimental

Synthesis and characterization of the fresh catalyst Pd–Ag (33–67) (1.9% Pd–3.7% Ag/$SiO_2$) are detailed in [22,23,25]. The experimental device and the measurement method of rates of the reactions involved in 1,2-dichloroethane hydrodechlorination are described in [24] and are briefly noted below.

### 2.1. Kinetic data acquisition

Reaction rates are measured in a fixed-bed tubular reactor in which a low composition change between inlet and outlet is maintained (differential reactor). The reactor is fed with the four compounds that have an influence on kinetics, that is 1,2-dichloroethane ($ClCH_2$–$CH_2Cl$), hydrogen ($H_2$), ethylene ($CH_2$=$CH_2$), and hydrogen chloride (HCl), diluted in helium. In addition to the rigorous differential reactor model which allows calculation of reliable reaction rates, the way to operate the reactor offers two particular advantages in a deactivation study. On the one hand, all catalyst pellets are identically deactivated along the reactor length since they are all in contact with the same compounds—reactants and products—at the same concentration and this allows a homogeneously modified catalyst sample for characterization to be obtained; on the second hand, that catalyst sample has been homogeneously deactivated in a differential reactor in the presence of significant amounts of reaction products which is more realistic from an industrial point of view. Note that ethane, which is the third product formed, is not introduced in the reactor feeding since it has been shown in [24] that it plays no role in the catalytic mechanism. It is then reasonable to assume that it also plays no role in deactivation.

For all kinetic measurements, the total pressure is maintained at 0.3 MPa (2.96 atm) and the total flow rate is fixed at 0.5 mmol $s^{-1}$. The temperature inside the reactor is successively fixed at 573, 596, and 647 K. The 6.2-cm-high catalytic bed is constituted of 0.25 g of Pd–Ag (33–67) catalyst pellets crushed and sieved between 250 and 500 μm. Prior to the measurement campaign, the catalyst was reduced in situ at atmospheric pressure in flowing $H_2$ (0.025 mmol $s^{-1}$) while being heated to 623 K at a rate of 350 K $h^{-1}$ and was maintained at this temperature for 3 h.

The net production rate of ethylene $r_E$ and the net production rate of ethane $r_A$ during hydrodechlorination of 1,2-dichloroethane are calculated from chromatographic measurements of $C_2H_4$ and $C_2H_6$ concentrations in the reactor effluent and from the differential reactor equation which is written as follows for ethylene and ethane net production,

$$r_E = \frac{F_E - F_{E0}}{W} \quad \text{and} \quad r_A = \frac{F_A}{W} \quad (F_{A0} = 0), \tag{1}$$

where $r_E$ = net ethylene production rate (mmol $kg^{-1}$ $s^{-1}$), $r_A$ = net ethane production rate (mmol $kg^{-1}$ $s^{-1}$), $F_E$ = molar flow rate of ethylene at the reactor outlet (mmol $s^{-1}$), $F_{E0}$ = molar flow rate of ethylene at the reactor inlet (mmol $s^{-1}$), $F_A$ = molar flow rate of ethane at the reactor outlet (mmol $s^{-1}$), $F_{A0}$ = molar flow rate of ethane at the reactor inlet (mmol $s^{-1}$), and $W$ = catalyst mass inside the reactor (kg).

Measurements of net ethylene production rate $r_E$ and net ethane production rate $r_A$ at 573, 596, and 647 K and for various partial pressures of 1,2-dichloroethane ($p_D$), hydrogen ($p_H$), ethylene ($p_E$), and hydrogen chloride ($p_{HCl}$) showed that a 1,2-dichloroethane hydrodechlorination reaction scheme can be represented by two reactions that are consecutive with regard to ethylene [24]. Those two reactions are hydrodechlorination of 1,2-dichloroethane into ethylene and undesired hydrogenation of ethylene into ethane:

$ClCH_2$–$CH_2Cl + H_2 \rightarrow CH_2$=$CH_2 + 2HCl$

(hydrodechlorination, rate $r_1$);

$CH_2$=$CH_2 + H_2 \rightarrow CH_3$–$CH_3$ (hydrogenation, rate $r_2$).

Hydrodechlorination rate $r_1$ and hydrogenation rate $r_2$ are obtained from mass balances:

$r_1 = r_E + r_A$,

hydrodechlorination rate = $ClCH_2$–$CH_2Cl$ consumption rate;

$r_2 = r_A$,

hydrogenation rate = $C_2H_6$ production rate.

Ethylene selectivity $S_E$ is given by $S_E = r_E/(r_E + r_A) = (r_1 - r_2)/r_1$.

Two measurement campaigns with two different loads of catalyst Pd–Ag (33–67) have been used to study deactivation. During the first campaign, the catalyst spent 80 h at 573 K inside the hydrodechlorination reactor whereas during the second campaign, it spent 662 h successively at 573, 596, and 647 K. This second campaign corresponds to the experimental data acquisition for the kinetic study presented in the previous paper of this series [24].

### 2.2. Regeneration and characterization of fresh, deactivated, and regenerated catalyst

At the end of the 662 h stay inside the hydrodechlorination reactor, the deactivated Pd–Ag (33–67) catalyst has been characterized in detail. Texture was analyzed by $N_2$ adsorption-desorption at 77 K. Metal particles were examined by X-ray diffraction (XRD), transmission electron microscopy (TEM), and carbon monoxide chemisorption

(CO) at 303 K. Palladium and silver contents were determined from inductively coupled plasma atomic emission spectroscopy (ICP-AES). Finally, the carbon content was measured by combustion with oxygen and the chlorine content was measured by combustion with sodium peroxide (see below).

Deactivated sample Pd–Ag (33–67) then underwent a regeneration treatment and the regenerated catalyst has been characterized by the same techniques as the deactivated one.

$N_2$ adsorption at 77 K and CO chemisorption at 303 K on the deactivated catalyst and regeneration treatment as well as $N_2$ adsorption at 77 K and CO chemisorption at 303 K on the regenerated catalyst were carried out with a single load of sample Pd–Ag (33–67). This load is introduced in a sample holder (Pyrex bulb) adapted on a Fisons Sorptomatic 1990 adsorption measurement device equipped with a turbomolecular vacuum pump which allows it to reach a high vacuum of $10^{-6}$ kPa. The Pyrex bulb is connected to two stopcocks which allow gases to flow through the catalytic bed for regeneration. During the various steps of regeneration and pretreatments for adsorption measurements, the sample holder is placed in temperature-programmed ovens. During adsorption measurements, it is plunged in a 77 K liquid $N_2$ bath for $N_2$ adsorption and in a 303 K thermostatically controlled water bath for CO adsorption.

The following method is applied: a 0.2054 g sample of deactivated Pd–Ag (33–67) catalyst is loaded in the sample holder and outgassed at $10^{-6}$ kPa at room temperature for 1 week. Sample holder is then plunged in a 77 K liquid $N_2$ bath and $N_2$ adsorption isotherm is measured. Sample is then outgassed, naturally reheated up to room temperature, and maintained under vacuum at $10^{-6}$ kPa for 6 h at the end of which it is plunged in a 303 K thermostatically controlled water bath. CO chemisorption isotherm is then determined at 303 K according to the method described in [23]: a first CO adsorption isotherm is achieved so as to measure the total amount of adsorbed carbon monoxide (chemisorbed + physisorbed). The catalyst is then outgassed on the measurements unit at 303 K during 2 h in a vacuum of $10^{-6}$ kPa and a second CO adsorption isotherm is measured in order to evaluate the amount of physisorbed CO. The chemisorption isotherm is obtained by subtracting the second isotherm from the first one.

At the end of the measurement of the second CO adsorption isotherm, the sample is outgassed at room temperature and then undergoes the regeneration treatment. This regeneration involves a calcination step and a reduction step. Under 0.037 mmol $s^{-1}$ flowing air, the catalyst is heated to 703 K at a rate of 120 K $h^{-1}$ and is maintained at this temperature during 16 h. It is then naturally cooled to room temperature and outgassed before hydrogen introduction. Under 0.037 mmol $s^{-1}$ flowing hydrogen, the catalyst is next heated to 673 K at a rate of 120 K $h^{-1}$ and is maintained at this temperature for 16 h. It is then naturally cooled to room temperature. The sample holder filled with hydrogen is next transferred on the outgassing unit where the catalyst is heated under vacuum to 613 K at a rate of 120 K $h^{-1}$, maintained at 613 K and $10^{-6}$ kPa for 16 h, and cooled naturally to room temperature.

The sample regenerated in this way is then submitted to $N_2$ adsorption at 77 K and CO adsorption at 303 K according to a procedure identical to the one described above for the deactivated catalyst. After the second CO adsorption isotherm, the catalyst is outgassed and recovered in order to continue its characterization by other methods.

Devices and handling of samples for characterization by XRD, TEM, and ICP-AES were described in the two first papers of this series [22,23].

The measurement of carbon content in deactivated and regenerated Pd–Ag (33–67) catalyst was carried out by combustion of carbonaceous residues at around 1200 K in a $O_2$–He mixture and measurement of the amount of $CO_2$ produced. The device is a Vario EL from Elementar equipped with a thermal conductivity detector (TCD) to analyze gases.

The amount of chlorine coming from chlorinated organic residues in the deactivated and regenerated Pd–Ag (33–67) catalyst was measured by combustion with sodium peroxide ($Na_2O_2$) in a Wurzschmitt bomb. Combustion reaction occurs explosively in an air-tight nickel bomb in presence of sodium peroxide and ethylene glycol for ignition. The organic Cl is converted in inorganic Cl in the form of sodium chloride NaCl. Combustion residues are dissolved in water and the chloride concentration is measured by potentiometric follow-up of the addition of a solution of silver nitrate causing chloride precipitation. Chlorine present in the form of AgCl in the sample is not measured.

## 3. Results

### 3.1. Kinetic data

Fig. 1b shows kinetic measures obtained under reference conditions that correspond to the center of the experimental design used for the kinetic study described in the previous paper of this series [24] (note that in [24], the rates were corrected with regard to the catalyst deactivation so as to all correspond to the same activity level). Fig. 1a shows kinetic measures at the center of a preliminary experimental design. This preliminary design is different from designs used in [24]. Operating conditions (partial pressures in 1,2-dichloroethane ($p_D$), hydrogen ($p_H$), ethylene ($p_E$), hydrogen chloride ($p_{HCl}$), and temperature) corresponding to the series of measures in Fig. 1a are thus different from those corresponding the series of measures in Fig. 1b. They are given in Table 1. Partial pressure values given in this table correspond to reactor inlet. Let us remember that partial pressures gaps between reactor inlet and outlet are low (differential reactor).

The series of measures in Fig. 1a shows activity and selectivity evolution during the first 80 h of catalyst operation, whereas the series in Fig. 1b gives activity and selectivity

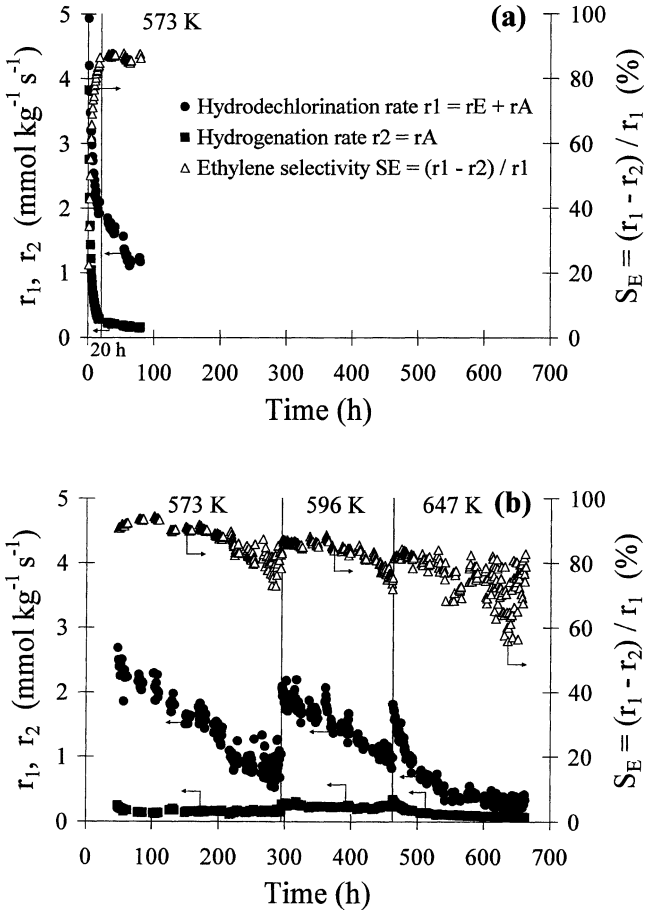


Fig. 1. Evolution of reaction rates and ethylene selectivity as a function of time. (a) First series of measurements; (b) second series of measurements.

Table 1
Operating conditions of both series of kinetic measurements

| Operating conditions | First series | Second series |
|---|---|---|
| $T$ (K) | 573 | 573, 596, 647 |
| $p_D$ (atm) | 0.059 | 0.148 |
| $p_H$ (atm) | 0.444 | 0.148 |
| $p_E$ (atm) | 0.015 | 0.016 |
| $p_{HCl}$ (atm) | 0.018 | 0.036 |

evolution between 48 and 662 h of operation. For the sake of simplicity, the data set of Fig. 1a will be named first series and the data set of Fig. 1b will be named second series.

During the first 20 h of catalyst operation in the first series, a very fast decrease of hydrodechlorination rate $r_1$ and hydrogenation rate $r_2$ is observed (Fig. 1a). Since $r_2$ decrease is faster than $r_1$ decrease, a considerable increase of ethylene selectivity $S_E = (r_1 - r_2)/r_1$ results: $S_E$ reaches nearly 90% after 20 h.

In the second series which gives reactions rates beyond 48 h of operation (Fig. 1b), one observes, as it already appears in the first series beyond 20 h, a decrease of hydrodechlorination rate $r_1$ that is faster than the decrease of hydrogenation rate $r_2$. As a result ethylene selectivity $S_E$ decreases. At 573 and 596 K, whereas hydrodechlorination rate $r_1$ clearly decreases, hydrogenation rate $r_2$ decreases only very weakly. At 647 K, the decrease of both rates is faster than at lower temperatures.

### 3.2. Characterization of fresh, deactivated, and regenerated Pd–Ag (33–67) catalyst

#### 3.2.1. Metal particles characterization

Fig. 2 shows the diffractograms of Pd–Ag (33–67) catalyst at different stages: fresh, deactivated after 662 h of operation in the hydrodechlorination reactor, and regenerated. Particles compositions and sizes calculated from those diffractograms are given in Table 2.

In Fig. 2, the diffractogram of fresh Pd–Ag (33–67) catalyst was already examined in the first paper of this series [22]. Between the (111) Bragg lines of pure palladium and silver, the fresh catalyst exhibits a broad peak which indicates the presence of a solid solution in the form of small Pd–Ag alloy particles. This solid solution gives also a broad peak between less intense (200) lines of Pd and Ag. However, this second peak appears clearly after spectrum deconvolution only (see example of deconvolution in [22]). The presence of unalloyed silver is clearly evident in the fresh catalyst, two peaks, (111) and (200), being characteristic of this metal. Composition and mean size of alloy particles were calculated [22] and are noted in Table 2. A bulk composition of 54 at% Pd–46 at% Ag and a size of 2 nm are obtained. For pure silver particles, a clearly higher size of 18 nm is obtained.

The diffractogram of deactivated Pd–Ag (33–67) catalyst allows detection of silver chloride (chlorargyrite) in the form of 20 nm particles (Table 2) only.

The diffractogram of regenerated Pd–Ag (33–67) catalyst shows that regeneration treatment allows restoration of alloy particles that were present in the fresh catalyst. Indeed, the broad diffraction peak located between (111) lines of pure Pd and pure Ag is found again which indicates the presence

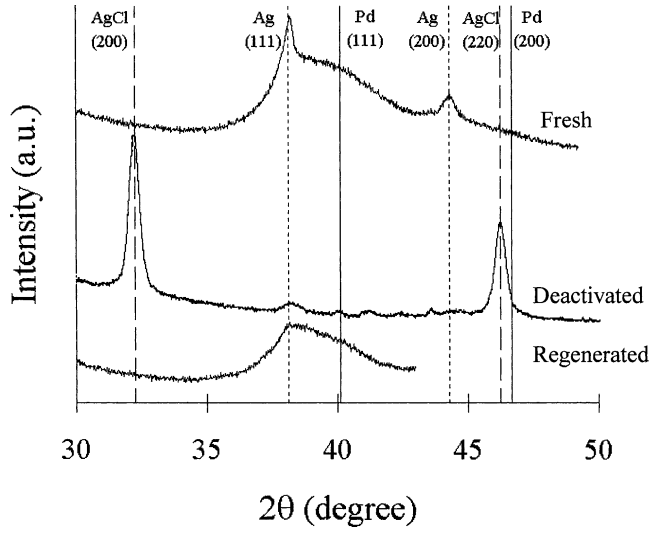


Fig. 2. X-ray diffraction patterns of Pd–Ag (33–67) catalyst.

Table 2
Characterization of metal particles in fresh, deactivated, and regenerated Pd–Ag (33–67) catalyst by XRD, TEM, and CO chemisorption

| Catalyst | Nature and composition of phases detected by XRD (at%) | | Particle size (nm) | | | | CO chemisorbed $n_{s,m}$ (mmol $g_{Pd}^{-1}$) |
|---|---|---|---|---|---|---|---|
| | | | XRD | | TEM | | |
| | Phase 1 | Phase 2 | Phase 1 | Phase 2 | Small | Large | |
| Fresh Pd–Ag (33–67) | 54% Pd–46% Ag | Ag | 2.0 | 18 | 3.0 | 10 | 0.66 |
| Deactivated Pd–Ag (33–67) | –[a] | AgCl | –[a] | 20 | 1.9 | 12 | 0.65 |
| Regenerated Pd–Ag (33–67) | 60% Pd–40% Ag | Ag | 2.0 | 6 | 3.0 | 12 | 0.80 |

[a] Not detected.

of a Pd–Ag solid solution. After subtraction of pure Ag (111) peak by means of deconvolution, examination of the broad peak corresponding to the solid solution leads to 2-nm particles with a 60 at% Pd–40 at% Ag composition that is a size and a composition nearly identical to those of alloy particles in the fresh catalyst. The pure silver (111) peak corresponds to a mean size of 6 nm.

TEM micrographs obtained at a magnification of $10^6$ of fresh, deactivated, and regenerated Pd–Ag (33–67) catalysts are shown in Figs. 3–5. Dark spots correspond to metal particles. Mean sizes of metal particles measured by TEM are given in Table 2. Let us note that, for the sake of simplicity, the term "metal particles" will still be used, although, in the deactivated catalyst, some particles could be constituted, at least in part, of metal chloride instead of metals.

As in the case of the fresh Pd–Ag (33–67) catalyst [22], microscopy analysis of deactivated and regenerated samples allows detection of metal particles that are distributed in two families of different size. These two families are clearly visible at a magnification of $2 \times 10^5$, an example of which is given in [22] with the fresh Pd–Ag (33–67) catalyst.

Mean sizes of large metal particles are similar in the fresh, deactivated, and regenerated catalyst and are around 10–12 nm. However, small metal particles exhibit mean sizes that are similar in the fresh and regenerated catalyst (3.0 nm), but that seem to be smaller in the deactivated catalyst (1.9 nm).

Isotherms of carbon monoxide chemisorption at 303 K on fresh, deactivated, and regenerated Pd–Ag (33–67) catalyst are presented in Fig. 6. The amounts of CO needed to form a monolayer chemisorbed on palladium sites, $n_{s,m}$, that are obtained by back-extrapolation [23,26–29] are given in Table 2. In order to avoid as much as one can a modification of the deactivated Pd–Ag (33–67) catalyst after its unloading from the hydrodechlorination reactor, the latter was outgassed at room temperature before CO adsorption measurements (see Experimental). Concerning the fresh and regenerated Pd–Ag (33–67) catalysts, they were outgassed at 613 K after the hydrogen treatment ([23] and Experimental).

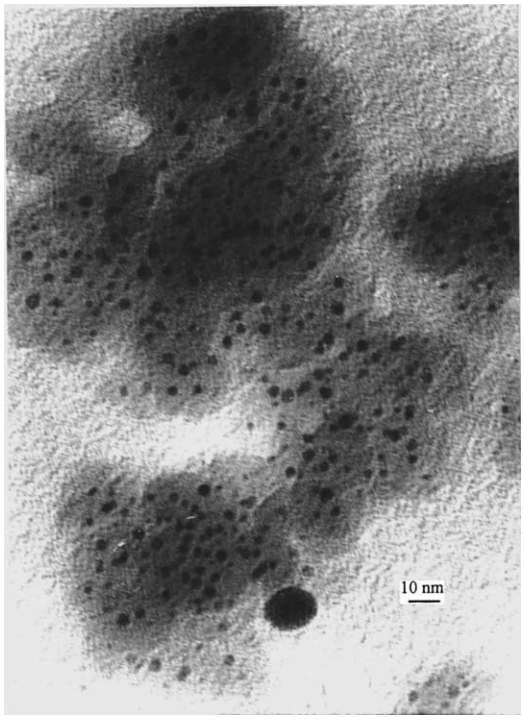


Fig. 3. TEM micrograph of fresh Pd–Ag (33–67) (original magnification, $\times 10^6$).

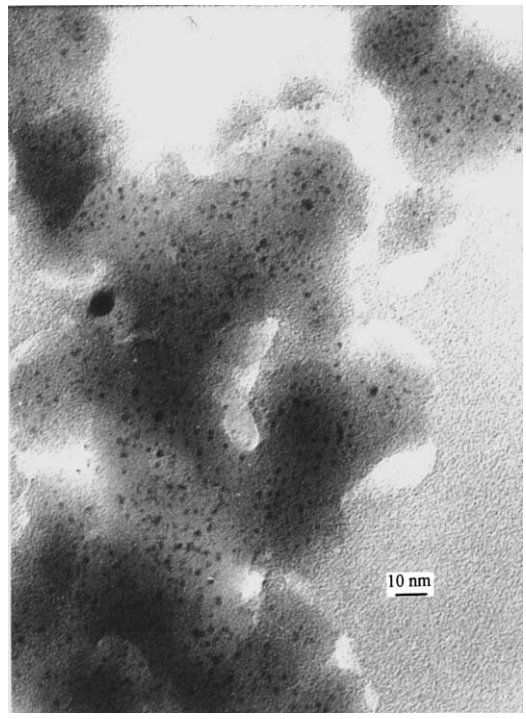


Fig. 4. TEM micrograph of deactivated Pd–Ag (33–67) (original magnification, $\times 10^6$).

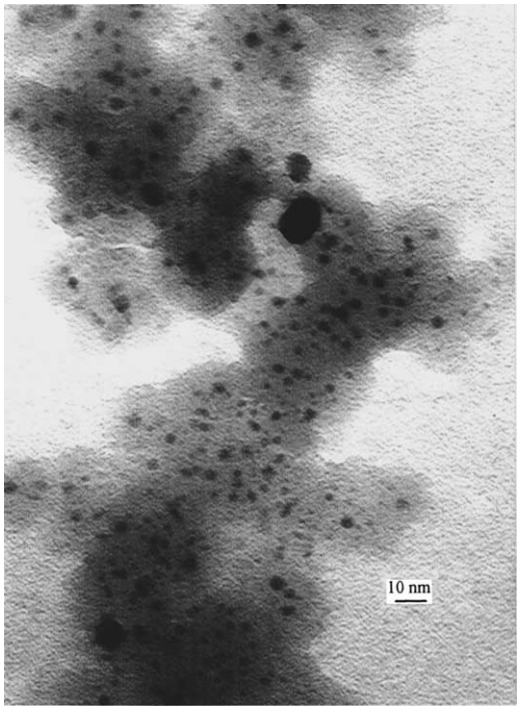


Fig. 5. TEM micrograph of regenerated Pd–Ag (33–67) (original magnification, $\times 10^6$).

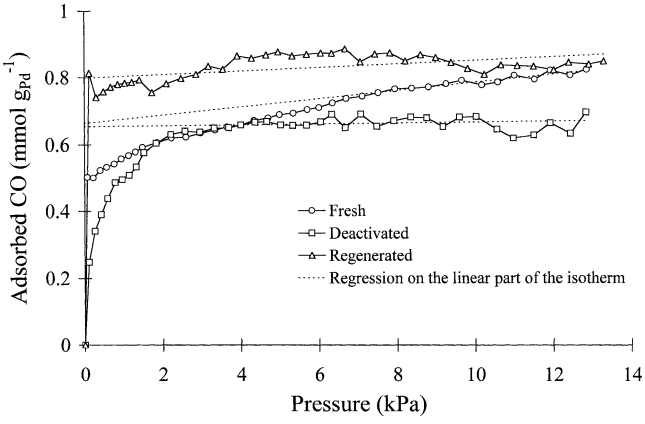


Fig. 6. CO chemisorption isotherms at 303 K of Pd–Ag (33–67) catalyst.

In the case of fresh and regenerated samples in which palladium is present in the form of Pd–Ag alloy particles as shown by XRD, it is admitted that CO is chemisorbed on palladium only [23]. In the case of deactivated sample, initial bimetallic particles were greatly modified but it will be still assumed that, as in the case of Pd–Ag alloy, CO chemisorption on the surface of those modified particles will still occur on palladium atoms only. For this reason, the amounts of chemisorbed CO are related to palladium mass that was measured by ICP-AES and that is the same in fresh, deactivated, and regenerated samples (see below).

Chemisorbed amounts $n_{s,m}$ given in Table 2 are quasi-identical for fresh (0.66 mmol $g_{Pd}^{-1}$) and deactivated (0.65 mmol $g_{Pd}^{-1}$) catalyst. The amount chemisorbed on regenerated sample is slightly higher (0.80 mmol $g_{Pd}^{-1}$). However, examination of Fig. 6 shows immediately that isotherms of deactivated and regenerated catalyst are less regular than that of fresh sample. The more pronounced instability of measurements with deactivated and regenerated samples is due to the lower mass of those samples available for chemisorption (about 0.2 g against 0.4 g for fresh catalyst). Chemisorbed amounts $n_{s,m}$ given by intersection with the $Y$-axis (uptake axis) of the regression line fitted on a linear-assumed region of deactivated and regenerated samples are characterized by a large error estimated at 0.10 mmol $g_{Pd}^{-1}$.

Table 3
Carbon and organic chlorine contents in deactivated and regenerated Pd–Ag (33–67) catalyst

| Catalyst | Carbon content ($g_C/g_{cata}$) | Organic chlorine content ($g_{organic\ Cl}/g_{cata}$) |
|---|---|---|
| Deactivated Pd–Ag (33–67) | 0.110 | 0.060 |
| Regenerated Pd–Ag (33–67) | 0.005 | 0.002 |

### *3.2.2. Quantitative determination of chlorinated organics and active metals*

Carbon and organic chlorine weight contents in deactivated and regenerated samples are given in Table 3.

Let us note that comparison between the weight increase of deactivated sample calculated from weighing (0.174 $g_{residues}/g_{cata}$) and the sum of carbon and organic chlorine contents (0.170 $g_{C+organic\ Cl}/g_{cata}$) shows that those two species form the main part of the residues mass in the deactivated catalyst. Contribution of inorganic chlorine in the form of AgCl and hydrogen masses to the overall residues mass is very low. Assuming that the whole silver in the catalyst is converted in AgCl, the maximum inorganic chlorine content is estimated at 0.012 $g_{inorganic\ Cl}/g_{cata}$.

It is observed that regeneration treatment allows elimination of almost the whole carbon and organic chlorine.

Active metals losses by formation and vaporization of metal chlorides in catalysts used for incineration of halogenated volatile organic compounds (VOC) have been already observed. For example, a copper oxide-based catalyst produces copper chloride which begins to evaporate beyond 723 K, thus leading to a considerable activity decrease [19]. Therefore, Pd–Ag (33–67) catalyst deactivation due to metal losses during hydrodechlorination is a conceivable possibility. So as to check this possibility, the palladium and silver contents were determined by ICP-AES in deactivated and regenerated samples and compared to the contents in the fresh catalyst (1.9% Pd–3.7% Ag/$SiO_2$). Values obtained with fresh, deactivated, and regenerated samples show that no metal losses occur during hydrodechlorination or during regeneration. In consequence, this possible deactivation cause can be rejected.

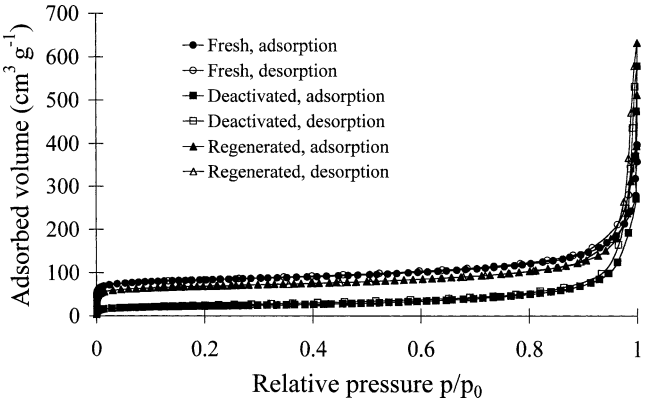


Fig. 7. $N_2$ adsorption-desorption isotherms at 77 K of Pd–Ag (33–67) catalyst.

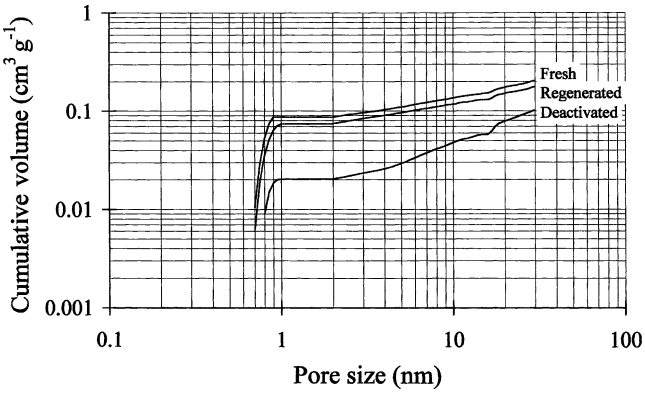


Fig. 8. Pore-size distributions of Pd–Ag (33–67) catalyst.

### 3.2.3. *Porous texture*

$N_2$ adsorption-desorption isotherms at 77 K of fresh, deactivated, and regenerated Pd–Ag (33–67) catalyst are presented in Fig. 7. The look of those isotherms was already discussed in [22]. Let us remember that they do not belong clearly to one of the five groups of the classification established by Brunauer et al. [30,31]. In the low-pressure region, a very fast increase of adsorbed volume is observed and is followed by a plateau, which corresponds to a type I isotherm characteristic of microporous solids. In the deactivated catalyst, this initial adsorption is much less important than in the fresh or regenerated one, which indicates that the deactivated sample contains less micropores than the fresh and regenerated ones as it will be confirmed by micropore volume values in the three samples (see below). As the saturation pressure $p_0$ approaches, adsorbed volume increases quickly again as in the case of type II or III isotherms corresponding to macroporous solids. Moreover, the three samples exhibit an hysteresis loop between adsorption and desorption which indicates $N_2$ capillary condensation in mesopores.

As already concluded in the case of fresh Pd–Ag (33–67) xerogel (1.9% Pd–3.7% Ag/$SiO_2$), and also in the case of Pd (100) (3.3% Pd/$SiO_2$), Pd–Ag (67–33) (2.2% Pd–1.1% Ag/$SiO_2$), Pd–Ag (50–50) (2.3% Pd–2.2% Ag/$SiO_2$), and Ag (100) (1.7% Ag/$SiO_2$) xerogels [22], deactivated and regenerated Pd–Ag (33–67) samples contain micropores (width $< 2$ nm), mesopores (2 nm $<$ width $<$ 50 nm), and macropores (width $>$ 50 nm) all at the same time [32].

Quantitative analysis results of $N_2$ adsorption isotherms at 77 K are given in Table 4. Cumulative pore-size distributions in fresh, deactivated, and regenerated Pd–Ag (33–67) catalysts have been calculated from $N_2$ adsorption isotherms at 77 K by combining Brunauer's method [33,34] applicable to micropores (width $< 2$ nm) with the Broekhoff–de-Boer method [35] applicable to mesopores smaller than 30 nm [22,31]. Those distributions are given in Fig. 8.

At the end of its stay in the hydrodechlorination reactor, it is observed that the catalyst has lost a considerable part of its specific surface area. Indeed, the BET surface area evolves from 321 $m^2\,g^{-1}$ for the fresh catalyst to 81 $m^2\,g^{-1}$ for the deactivated one (Table 4).

As explained previously in detail [22], $t$-plots (adsorbed volume as a function of adsorbed $N_2$ layer thickness, $t$) of catalysts Pd (100), Pd–Ag (67–33), Pd–Ag (50–50), and Pd–Ag (33–67) are similar (see Fig. 9 (fresh) as well as Fig. 10 in [22]). They always exhibit a sharp downward deviation at around $t = 0.4$ nm, which corresponds to filling of micropores characterized by a very narrow size distribution centered on $2t = 0.8$ nm, followed by an upward deviation due to capillary condensation in mesopores. The micropore-size distribution is then calculated by Brunauer's method applied to the downward deviation. The result of that calculation in the case of fresh Pd–Ag (33–67) catalyst is given in Fig. 8 in the microporous domain, that is for sizes lower than 2 nm. A steep volume increase is observed at around 0.8 nm followed by a plateau, which corresponds indeed to a narrow micropore-size distribution.

Table 4
Texture of fresh, deactivated, and regenerated Pd–Ag (33–67) catalyst

| Catalyst | $S_{BET}$ ($m^2\,g^{-1}$) | $S_t$ ($m^2\,g^{-1}$) | $S_w$ ($m^2\,g^{-1}$) | $S_{micro}$ ($m^2\,g^{-1}$) | $V_{micro}$ ($cm^3\,g^{-1}$) | $V_{2-30}$ ($cm^3\,g^{-1}$) |
|---|---|---|---|---|---|---|
| Fresh Pd–Ag (33–67) | 321 | 322 | 98 | 224 | 0.087 | 0.117 |
| Deactivated Pd–Ag (33–67) | 81 | 82 | 58 | 24 | 0.020 | 0.081 |
| Regenerated Pd–Ag (33–67) | 261 | 262 | 96 | 166 | 0.074 | 0.103 |

$S_{BET}$, specific surface area obtained by the BET method; $S_t$, specific surface area obtained from the slope before the downward deviation in the $t$-plot; $S_w$, specific surface area obtained from the slope after the downward deviation in the $t$-plot; $S_{micro} = S_t - S_w$; $V_{micro}$, specific micropore volume calculated by Brunauer's method; $V_{2-30}$, volume of mesopores between 2 and 30 nm calculated by the Broekhoff–de-Boer method [27].

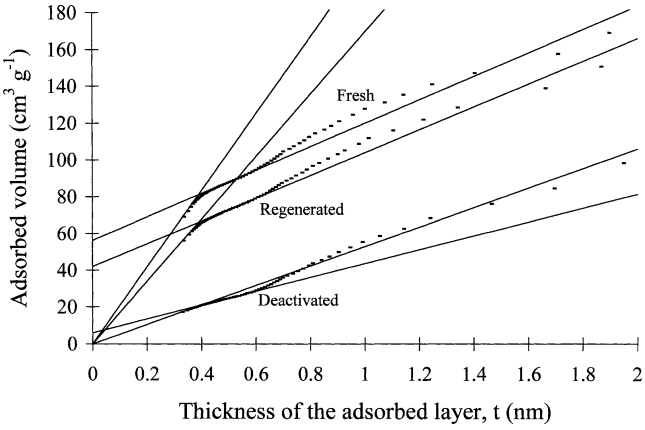


Fig. 9. $t$-plots of Pd–Ag (33–67) catalyst.

It is interesting to note that deactivated and regenerated catalyst exhibits $t$-plots, and therefore micropore-size distributions, that are very similar to those of fresh catalyst (Figs. 8 and 9). After operation in the hydrodechlorination reactor as well as after regeneration, a narrow micropore-size distribution centered around 0.8 nm is still observed. Only volumes corresponding to those micropores, $V_{\text{micro}}$, are modified (Table 4). Micropore volume of deactivated catalyst ($V_{\text{micro}} = 0.020$ cm$^3$ g$^{-1}$) is clearly lower than the one of fresh catalyst ($V_{\text{micro}} = 0.087$ cm$^3$ g$^{-1}$) and regeneration allows recovery of most of the lost volume ($V_{\text{micro}} = 0.074$ cm$^3$ g$^{-1}$).

Let us clarify the meaning of surface areas $S_t$, $S_w$, and $S_{\text{micro}}$ whose values are given in Table 4. In $t$-plots of fresh, deactivated, and regenerated Pd–Ag (33–67) catalyst (Fig. 9), slopes on either side of the downward deviation, but before the upward deviation, allow calculation of $S_t$, which is almost equal to $S_{\text{BET}}$ and $S_w$. As $S_{\text{BET}}$, $S_t$ is an estimate of the total surface area accessible for nitrogen inside the porous solid. $S_w$ is calculated from the slope after the downward deviation in the $t$-plot, that is, after the disappearance of micropores by filling with nitrogen. Therefore, $S_w$ corresponds to the surface developed by mesopores and macropores (size $> 2$ nm), that is, to the external surface of $SiO_2$ microporous particles in which bimetallic particles active for hydrodechlorination are trapped [22]. $S_{\text{micro}}$ is equal to $S_t - S_w$ and so corresponds to the surface of micropores located inside silica particles.

Since the size of micropores in the fresh, deactivated, and regenerated Pd–Ag (33–67) catalyst remains roughly constant, the microporous surface area, $S_{\text{micro}}$, evolves in parallel with the microporous volume, $V_{\text{micro}}$ (Table 4). Microporous surface areas obtained with fresh, deactivated, and regenerated samples are 224, 24, and 166 m$^2$ g$^{-1}$, respectively.

The surface developed by mesopores and macropores, $S_w$, is lower in the deactivated catalyst ($S_w = 58$ m$^2$ g$^{-1}$) than in the fresh one ($S_w = 98$ m$^2$ g$^{-1}$), but it is entirely recovered after regeneration ($S_w = 96$ m$^2$ g$^{-1}$). In the mesoporous domain examined (2 nm $<$ size $<$ 30 nm), the three samples exhibit a continuous pore-size distribution (Fig. 8). The volume of those mesopores, $V_{2-30}$, is given in Table 4.

## 4. Discussion

As noted in the Introduction, the causes of catalyst deactivation during hydrodechlorination reactions that are generally suggested are metal poisoning by chlorine [4–9], coking [5,6,10–18], loss of metal due to formation of volatile chlorides [19], and metal sintering [8,19–21]. Note that, concerning the latter, in some cases the presence of chlorinated compounds can produce the opposite effect, that is, an increase of metal dispersion [6,11,16,17,20,36,37].

The performances of monometallic palladium catalysts have been studied in various hydrodechlorination reactions. Moulijn and co-workers studied extensively hydrodechlorination of $CCl_2F_2$ and $CCl_3F$ over a 1 wt% Pd/C catalyst and the associated activity and selectivity changes [6,15–17]. Ordonez et al. studied hydrodechlorination of $C_2Cl_4$ over a 0.5 wt% Pd/C [13]. In some cases, under appropriate temperature and feed composition conditions, the catalyst performances were stable for a very long operation time [15,16]. When observed, the deactivation was attributed to the formation of carbonaceous deposits on the catalyst surface.

Among the four possible deactivation causes presented above, the loss of metal and the sintering of metal particles can be eliminated as shown by ICP-AES—same Pd and Ag contents in fresh, deactivated, and regenerated catalysts—and TEM—no increase of metal particle size—results, respectively (Figs. 3 and 4 and Table 2).

Let us then examine the two last possible deactivation causes: poisoning of metallic active sites by chlorine and coking, that is, deposit of halogenated carbonaceous residues on metal and support.

CO chemisorption indicates that the amount chemisorbed by the fresh catalyst ($n_{s,m} = 0.66$ mmol $g_{Pd}^{-1}$) is close to the amount chemisorbed by the deactivated catalyst ($n_{s,m} = 0.65$ mmol $g_{Pd}^{-1}$) (Table 2). If it is admitted for deactivated Pd–Ag (33–67) catalyst that, as for fresh Pd–Ag (33–67) catalyst, CO chemisorption occurs on palladium only and that chemisorption stoichiometry $X_{Pd-CO}$, which is the mean number of Pd atoms on which one CO molecule is adsorbed, is equal to 1 [23], the result of CO chemisorption indicates that the number of Pd atoms that are accessible for the gaseous phase in the deactivated Pd–Ag (33–67) catalyst seems not to have been altered significantly in relation to the fresh Pd–Ag (33–67) catalyst.

In consequence, CO chemisorption results suggest that palladium is neither poisoned by chlorine because of irreversible adsorption, nor made inaccessible because of covering by chlorinated carbonaceous residues or fouling of pores leading to bimetallic particles (coking). Moreover, those results support the hypothesis, already suggested by TEM, that no Pd–Ag bimetallic particles sintering occurs. The occur-

rence of a possible palladium redispersion due to the presence of chlorinated compounds seems also unlikely.

If one confines oneself to the list of possible deactivation causes presented above, we have then to consider a deactivation of Pd–Ag (33–67) catalyst which would result from the disappearance of silver sites either by poisoning or by covering by chlorinated carbonaceous residues. Is such a deactivation mechanism in agreement with kinetic data and results of fresh, deactivated, and regenerated Pd–Ag (33–67) catalyst characterization presented in the previous section? This question is discussed below.

Let us first examine the compatibility of a deactivation mechanism due to silver sites disappearance with kinetic data in Fig. 1b and Fig. 1a after the first 20 operating hours during which ethylene selectivity, $S_E$, increases very quickly from about 20 to 90%. Those data show a decrease of the hydrodechlorination rate, $r_1$, which is faster than the decrease of the hydrogenation rate, $r_2$. As a result, the ethylene selectivity, $S_E$, decreases.

According to the results of the kinetic study presented in the third paper of the present series [24], hydrodechlorination and hydrogenation take place according to a sequence of elementary steps in which the step determining the hydrodechlorination rate $r_1$, rds1, and the step determining the hydrogenation rate $r_2$, rds2, are respectively,

$$ClCH_2CH_2Cl + 2s_1 \rightarrow ClCH_2CH_2s_1 + Cls_1 \quad \text{rds1},$$

$$C_2H_5s_1 + Hs_2 \rightarrow C_2H_6 + s_1 + s_2 \quad \text{rds2}.$$

Since sites $s_1$ and $s_2$ have been identified with silver sites and palladium sites, respectively [24], the step determining the hydrodechlorination rate, rds1, requires two silver sites whereas the step determining the hydrogenation rate, rds2, requires one silver site and one palladium site (note that such a mechanism is in agreement with a recent study on 1,2-dichloroethane hydrodechlorination catalyzed by Pt–Cu/$SiO_2$ catalysts [38], that is, bimetallic catalysts that contain a metal from group VIII combined with a metal from group Ib, as in Pd–Ag/$SiO_2$ catalysts). Therefore, if it is admitted that, during operation in the hydrodechlorination reactor, palladium sites remain unaltered, as suggested above, and that silver sites disappear either by chlorine poisoning or by covering by chlorinated carbonaceous residues, a decrease of the hydrodechlorination rate, $r_1$, which is faster than the decrease of the hydrogenation rate, $r_2$, can be expected. It can then be concluded that a deactivation mechanism due to silver sites disappearance is not inconsistent with kinetic data in Fig. 1b and kinetic data after the first 20 operating hours in Fig. 1a.

On the other hand, that mechanism alone does not allow us to explain the Pd–Ag (33–67) catalyst deactivation during the first 20 operating hours of the first series of kinetic measurements (Fig. 1a). Indeed, during that period, an increase of ethylene selectivity $S_E = (r_1 - r_2)/r_1$ is observed which results from an initial decrease of the hydrogenation rate $r_2$ which is faster than the initial decrease of the hydrodechlorination rate $r_1$, which seems to be inconsistent with a deactivation resulting from the disappearance of silver sites. During those very first operating hours, an additional phenomenon probably occurs, but the available experimental results do not allow identification of that phenomenon.

Let us now examine X-ray diffraction and transmission electron microscopy results. According to XRD analysis, the large pure silver particles in the fresh Pd–Ag (33–67) catalyst have been converted into silver chloride particles with comparable size in the deactivated Pd–Ag (33–67) catalyst (Table 2). According to the kinetic study in [24], chlorine atoms coming from 1,2-dichloroethane and hydrogen chloride become adsorbed on the silver surface. Without palladium which supplies hydrogen atoms for the regeneration of the chlorinated silver surface into metallic Ag, silver sites are rapidly deactivated. Let us remember that Ag (100) pure silver catalyst (1.7% Ag/$SiO_2$) is completely inactive from the first measurement after 0.5 h operation during the evaluation test [22]. Once adsorbed, chlorine atoms can diffuse inside the bulk of silver particles and form finally bulk silver chloride particles observed by XRD, the size of which is consistent with large particles detected by TEM.

On the surface of small bimetallic particles, despite the presence of palladium which is used to eliminate chlorine atoms adsorbed on silver during hydrodechlorination and which remains unaltered according to CO chemisorption results, the deactivation mechanism corresponding to silver sites disappearance suggests, in addition to the possible deposit of chlorinated carbonaceous residues on those silver sites, the gradual formation of a stable silver chloride. Moreover, as in pure silver particles, chlorine atoms can probably diffuse inside the bulk of alloy particles and form chlorides in them as well. Active bimetallic particles would therefore be transformed into a blend which can be composed of metallic Pd, metallic Ag, and AgCl at the surface as well as palladium and silver in the form of metals or chlorides in the bulk. Consequently, it would not be surprising that the initial crystal structure of those nanoparticles is transformed into an amorphous structure which does not diffract X-rays anymore, which would explain that they are not detected by XRD. Their density would change as well and this could modify their contrast in electron microscopy by comparison with the silica support (partially covered with halogenated carbonaceous residues) and give the impression that their size has decreased as indicated by the mean sizes obtained by TEM (Table 2).

During catalyst operation in the hydrodechlorination reactor, it seems then that Pd–Ag alloy particles and pure Ag particles are gradually loaded with chlorine. According to XRD and TEM characterization results of the regenerated catalyst, regeneration allows a complete removal of chlorine in metal particles since initial particles of the fresh catalyst are roughly recovered.

It is interesting at this point to comment on the difference in deactivation behaviors between pure Pd and bimetallic Pd–Ag hydrodechlorination catalysts. As noted above, Moulijn and co-workers [6,15–17] and Ordonez

et al. [13] attributed the deactivation of Pd/C catalysts during hydrodechlorination of $CCl_2F_2$, $CCl_3F$, and $C_2Cl_4$ to the formation of carbonaceous deposits on the catalyst surface. Poisoning was concluded to be not important. In the present study, experimental results suggest that deactivation of the Pd–Ag/$SiO_2$ catalyst during hydrodechlorination of $ClCH_2$–$CH_2Cl$ would be due to the disappearance of silver sites either by the gradual formation of a stable surface silver chloride or by the deposit of chlorinated carbonaceous residues on those silver sites, or most probably by both mechanisms. On the other hand, palladium sites would remain intact. It has been shown in the first paper of this series [22] that the addition of Ag in a Pd/$SiO_2$ sample stabilizes the catalyst toward deactivation during hydrodechlorination screening tests. That stabilization effect was confirmed recently by Arsenault and Gonzalez [39] in the case of Pd–Cu/$SiO_2$ catalysts also used for selective hydrodechlorination of 1,2-dichloroethane into ethylene: besides the selectivity effect, the addition of the group IB metal has the additional advantage of decreasing the deactivation of the catalyst. Therefore, it appears clearly that alloying Pd with a IB metal modifies the deactivation mechanism during hydrodechlorination. A comparison between catalytic performances of catalyst Pd–Ag (33–67) obtained during the screening test presented in [22] and during both measurement campaigns presented in Fig. 1 in the present paper indicates that whereas stable activity and selectivity are obtained in the screening test, a clear deactivation is observed in Fig. 1. The main difference between catalytic measurements in the present study and in [22] is the introduction of reaction products (HCl and $CH_2{=}CH_2$) in the feeding flow of the reactor in the present study, whereas the reactor is fed with the chlorinated organic compound (here, $ClCH_2$–$CH_2Cl$) and $H_2$ only in [22], as in most hydrodechlorination studies. This suggests that hydrogen chloride and/or ethylene induce a marked deactivation. The deactivation of the catalyst by HCl can be explained by its ability to chlorinate the active metallic sites and thus to transform them into stable surface chlorides. Since chlorine is more strongly linked with silver than with palladium [24] and since, contrary to Pd, Ag cannot adsorb hydrogen directly to remove adsorbed chlorine [24], it is not surprising that silver sites are deactivated by chlorine poisoning whereas Pd sites remain intact. Concerning the deactivation by ethylene, it has been shown in [24] that, during hydrodechlorination of 1,2-dichloroethane over the Pd–Ag (33–67) catalyst, $CH_2{=}CH_2$ as well as $ClCH_2$–$CH_2Cl$ adsorb on silver partially covered with chlorine atoms but not on palladium atoms that are individually isolated in the silver matrix [23,40]. Those adsorptions can become the starting point of coking on silver active sites by formation of carbonaceous heavy residues from the carbonaceous adsorbed species. With such a mechanism, Pd sites remain intact as indicated by CO chemisorption. In the case of pure Pd catalysts, as Pd/$SiO_2$ sample (Pd (100)) in [22] or Pd/C catalysts used by Moulijn and co-workers [6,15–17] and Ordonez et al. [13], since Pd is the only active metal, the chlorinated organic reactant ($ClCH_2$–$CH_2Cl$ in [22], $CCl_2F_2$ in [6,15,16], $CCl_3F$ in [17], or $C_2Cl_4$ in [13]) as well as the carbonaceous products formed adsorb on that metal which can thus undergo a deactivation by coking. Moreover, it is possible that poisoning by chlorine does not occur with pure Pd catalysts since chlorine atoms are easily removed by combination with hydrogen atoms adsorbed on the same metal.

Concerning catalyst texture evolution, it seems that the partial disappearance of pores because of their fouling by chlorinated carbonaceous residues does not decrease the number of bimetallic particles that are accessible for the gaseous phase since, according to CO chemisorption results, the number of accessible palladium atoms is approximately the same in the fresh and in the deactivated catalyst. The fact that accessibility does not decrease is probably a consequence of the large number of pores, that is, of different ways, leading to the same active bimetallic particle inside the particular structure of cogelled catalysts examined in this study [22,41,42]. The disappearance of some number of ways leading to one particle does not alter its accessibility.

## 5. Conclusions

According to the comparison between physico-chemical properties of Pd–Ag (33–67) catalyst before and after operation in the hydrodechlorination reactor, a deactivation whose main cause would be a disappearance of silver sites present at the surface of active bimetallic particles seems to be plausible. That disappearance would be due to the formation of a stable silver chloride and possibly also to the covering of silver sites with chlorinated carbonaceous residues. On the contrary, palladium sites would remain intact.

After an initial period of a few hours, the evolution of hydrodechlorination and hydrogenation rates is not inconsistent with such a mechanism. Indeed, a decrease of the hydrodechlorination rate which is faster than the decrease of the hydrogenation rate is observed which could be explained by the disappearance of silver sites since the step determining the hydrodechlorination rate requires two silver sites whereas the step determining the hydrogenation rate requires only one.

The initial period of catalyst operation is characterized by a much faster drop of both reaction rates. During that period of catalyst quick evolution, the hydrogenation rate decreases faster than the hydrodechlorination rate, which cannot be explained by the mechanism based on silver site disappearance alone. During those first operation hours, an additional phenomenon probably occurs which cannot be identified with the available experimental results.

The analysis of the regenerated catalyst shows that the regeneration treatment including an oxidation step followed by a reduction step, allows restoration of initial metal particles as well as the major part of porosity (whose partial disappearance seems not to alter catalyst activity).

## Acknowledgments

The authors are very grateful to Mr. C. Lebrun from the Solvay Company for his invaluable assistance during the kinetic data acquisition. B. Heinrichs thanks the Fonds pour la Formation à la Recherche dans l'Industrie et dans l'Agriculture, F.R.I.A., for a PhD grant. The Ministère de la Région Wallonne, the Ministère de la Communauté Française de Belgique, and the Belgian F.N.R.S. are also gratefully acknowledged for financial support.

## References

[1] G.F. Froment, K.B. Bischoff, Chemical Reactor Analysis and Design, Wiley, New York, 1990.
[2] D.L. Trimm, in: G. Ertl, H. Knözinger, J. Weitkamp (Eds.), Handbook of Heterogeneous Catalysis, Vol. 3, Wiley–VCH, Weinheim, 1997, p. 1263.
[3] J.B. Butt, in: J.R. Anderson, M. Boudart (Eds.), Catalysis: Science and Technology, Vol. 6, Springer, Berlin, 1984, p. 1.
[4] B. Coq, G. Ferrat, F. Figueras, J. Catal. 101 (1986) 434.
[5] J.W. Bozzelli, Y.-M. Chen, S.S.C. Chuang, Chem. Eng. Commun. 115 (1992) 1.
[6] A. Wiersma, E.J.A.X. van de Sandt, M.A. den Hollander, H. van Bekkum, M. Makkee, J.A. Moulijn, J. Catal. 177 (1998) 29.
[7] A. Malinowski, W. Juszczyk, M. Bonarowska, J. Pielaszek, Z. Karpinski, J. Catal. 177 (1998) 153.
[8] A. Gampine, D.P. Eyman, J. Catal. 179 (1998) 315.
[9] Y.H. Choi, W.Y. Lee, Catal. Lett. 67 (2000) 155.
[10] S.Y. Kim, H.C. Choi, O.B. Yanga, K.H. Lee, J.S. Lee, Y.G. Kim, J. Chem. Soc., Chem. Commun. (1995) 2169.
[11] W. Zhu, J. Zhang, F. Kapteijn, M. Makkee, J.A. Moulijn, Stud. Surf. Sci. Catal. 139 (2001) 21.
[12] K.A. Frankel, J.J. Spivey, G.W. Roberts, Stud. Surf. Sci. Catal. 139 (2001) 439.
[13] S. Ordonez, F.V. Diez, H. Sastre, Appl. Catal. B 31 (2001) 113.
[14] K.A. Frankel, B.W.-L. Jang, G.W. Roberts, J.J. Spivey, Appl. Catal. A 209 (2001) 401.
[15] A. Wiersma, E.J.A.X. van de Sandt, M. Makkee, H. van Bekkum, J.A. Moulijn, Stud. Surf. Sci. Catal. 101 (1996) 369.
[16] A. Wiersma, E.J.A.X. van de Sandt, M. Makkee, J.A. Moulijn, Appl. Catal. A 212 (2001) 223.
[17] S. Ordonez, M. Makkee, J.A. Moulijn, Appl. Catal. B 29 (2001) 13.
[18] K.A. Frankel, B.W.-L. Jang, J.J. Spivey, G.W. Roberts, Appl. Catal. A 205 (2001) 263.
[19] N. Mastrell, Info. Chim. 396 (1998) 89.
[20] E.D. Boyes, D.R. Coulson, G.W. Coulston, M.P. Diebold, P.L. Gai, G.A. Jones, C.S. Kellner, J.J. Lerou, L.E. Manzer, P.L. Mills, V.N.M. Rao, Proc. Am. Chem. Soc. Division Petrol. Chem. 38 (1993) 847.
[21] Z. Ainbinder, L.E. Manzer, M.J. Nappa, in: G. Ertl, H. Knözinger, J. Weitkamp (Eds.), Handbook of Heterogeneous Catalysis, Vol. 4, Wiley–VCH, Weinheim, 1997, p. 1677.
[22] B. Heinrichs, P. Delhez, J.-P. Schoebrechts, J.-P. Pirard, J. Catal. 172 (1997) 322.
[23] B. Heinrichs, F. Noville, J.-P. Schoebrechts, J.-P. Pirard, J. Catal. 192 (2000) 108.
[24] B. Heinrichs, J.-P. Schoebrechts, J.-P. Pirard, J. Catal. 200 (2001) 309.
[25] P. Delhez, B. Heinrichs, J.-P. Pirard, J.-P. Schoebrechts, US patent 6,072,096, 2000.
[26] J.R. Anderson, Structure of Metallic Catalysts, Academic Press, London, 1975.
[27] G. Bergeret, P. Gallezot, in: G. Ertl, H. Knözinger, J. Weitkamp (Eds.), Handbook of Heterogeneous Catalysis, Vol. 2, Wiley–VCH, Weinheim, 1997, p. 439.
[28] E. Iglesia, M. Boudart, J. Catal. 81 (1983) 204.
[29] D. Cormack, J. Pritchard, R.L. Moss, J. Catal. 37 (1975) 548.
[30] S. Brunauer, L.S. Deming, W.S. Deming, E. Teller, J. Am. Chem. Soc. 62 (1940) 1723.
[31] A.J. Lecloux, in: J.R. Anderson, M. Boudart (Eds.), Catalysis: Science and Technology, Vol. 2, Springer, Berlin, 1981, p. 171.
[32] J. Rouquerol, D. Avnir, C.W. Fairbridge, D.H. Everett, J.H. Haynes, N. Pernicone, J.D.F. Ramsay, K.S.W. Sing, K.K. Unger, Pure Appl. Chem. 66 (1994) 1739.
[33] R.S. Mikhail, S. Brunauer, E.E. Bodor, J. Colloid Interface Sci. 26 (1968) 45, 54.
[34] S. Brunauer, Chem. Eng. Progr. Symp. Ser. No. 96 65 (1969) 1.
[35] J.C.P. Broekhoff, J.H. de Boer, J. Catal. 9 (1967) 8.
[36] M.J. D'Aniello Jr., D.R. Monroe, C.J. Carr, M.H. Krueger, J. Catal. 109 (1988) 407.
[37] O.C. Feeley, W.M.H. Sachtler, Appl. Catal. 75 (1991) 93.
[38] V.Y. Borovkov, D.R. Luebke, V.I. Kovalchuk, J.L. d'Itri, J. Phys. Chem. B 107 (2003) 5568.
[39] S. Arsenault, R.D. Gonzalez, in: 18th North American Catalysis Society Meeting, Technical Program, Cancun, June 1–6, 2003, Nat. Sci. Foundation, North Am. Catal. Society, 2003, p. 63.
[40] G.A. Kok, A. Noordermeer, B.E. Nieuwenhuys, Surf. Sci. 152/153 (1985) 505.
[41] B. Heinrichs, F. Noville, J.-P. Pirard, J. Catal. 170 (1997) 366.
[42] B. Heinrichs, J.-P. Pirard, J.-P. Schoebrechts, AIChE J. 47 (2001) 1866.